Journal of Solid State Chemistry 188 (2012) 92–99

Contents lists available at SciVerse ScienceDirect

Journal of Solid State Chemistry

journal homepage: www.elsevier.com/locate/jssc

Structural variation and optical properties of ZnO–$LiGaO_2$ pseudo-binary system

Takahisa Omata [a,*], Masao Kita [b], Kosuke Tachibana [a], Shinya Otsuka-Yao-Matsuo [a]

[a] Division of Materials and Manufacturing Science, Graduate School of Engineering, Osaka University, 2-1 Yamada-oka, Suita 565–0871, Japan
[b] Department of Ecomaterials Engineering, Toyama National College of Technology, 13 Hongo-machi, Toyama 939-8630, Japan

ARTICLE INFO

Article history:
Received 24 November 2011
Received in revised form
22 January 2012
Accepted 24 January 2012
Available online 31 January 2012

Keywords:
Zinc oxide
Lithium gallium oxide
I–III–V_2 semiconductor
Phase transformation
Energy band gap
Wide band gap semiconductors

ABSTRACT

The structural variation in the $x(LiGaO_2)_{1/2}(1-x)ZnO$ alloy system was studied by powder XRD, TEM-SAD and Raman spectroscopy. It was elucidated that the phase varied upon increasing the alloying level was the wurtzite-type for $0 \le x < 0.2$, the Zn_2LiGaO_4-type for $0.2 \le x \le 0.5$ and the β-$LiGaO_2$-type for $0.8 \le x \le 1$, and the $0.5 < x < 0.8$ region was the immiscible region of ZnO with $LiGaO_2$. The solubility limit of $LiGaO_2$ in ZnO was explained by the c_0/a_0 ratio based on the fact that there is no binary wurtzite phase for a c_0/a_0 less than 1.6. The optical phonons of wurtzite and its derived phase were simply explained by the lattice shrinkage and reduced mass upon reduction the alloying of ZnO with $LiGaO_2$. The bowing parameter of the optical band gap of $y(Zn_2LiGaO_4)_{1/4}(1-y)ZnO$ was determined to be 0.67 eV. The value was very low, and it was related to the small lattice and chemical mismatches between the Zn_2LiGaO_4 and ZnO.

1. Introduction

Zinc oxide (ZnO) is a direct semiconductor oxide possessing a wide band gap (3.37 eV) and large exciton binding energy (60 meV) [1]. These very attractive physical properties enable its use as a material for light-emitting devices in the ultraviolet (UV) region and transparent electrodes for visible (Vis) light. The higher abundance of zinc in natural resources than indium and gallium for nitride semiconductors of (In,Ga)N has also recently received attention in addition to the above mentioned physical properties.

In order to use ZnO in light-emitting devices, adjusting its energy band gap, i.e., band gap engineering, is generally required. Band gap engineering is usually conducted by the alloying of ZnO with MgO for band gap widening and with CdO for band gap narrowing [2, 3]. However, the controllable region is limited, because their alloying regions are limited due to the structural difference between the wurtzite-type hexagonal ZnO and the rock-salt-type cubic MgO and CdO. When we get oxide semiconductors that are applicable to the band gap engineering of ZnO, the ZnO is expected to have broader applications. Based on this perspective, we have investigated the alloying of ZnO with β-$LiGaO_2$ that possesses a wurtzite-derived structure and wide band gap of 5.6 eV [4]. A new quaternary oxide semiconductor, Zn_2LiGaO_4, with a wurtzite-derived structure was recently discovered [5, 6], and the alloys $x(LiGaO_2)_{1/2}(1-x)ZnO$ were successfully obtained in the region of $x \le 0.5$ for the bulk and thin films [7].

On the other hand, the $x(LiGaO_2)_{1/2}(1-x)ZnO$ alloy system is attractive from a structural aspect. There are many structural studies of alloyed semiconductors of III–V or II-chalcogen systems. Among them, the alloy systems of the simple zincblende phase with the cation-ordered chalcopyrite phase, such as the ZnS–$CuInS_2$ alloy system, are involved [8–14]. However, such studies have not been demonstrated in oxide semiconductors until now; the studies have been limited to the simple wurtzite phase, such as the MgO–ZnO and BeO–ZnO alloy systems [2, 15].

In the present paper, the structural variation of the $x(LiGaO_2)_{1/2}(1-x)ZnO$ over a whole pseudo-binary composition range by the X-ray diffraction (XRD) and selected area electron diffraction (SAD) was first investigated. The obtained results were discussed based on a comparison with the MgO–ZnO system. The optical properties of the Raman spectra and optical band gap depending on the alloying level were studied.

2. Experimental

$x(LiGaO_2)_{1/2}(1-x)ZnO$ semiconductor alloys were prepared by a solid state reaction between β-$LiGaO_2$ and ZnO. The starting β-$LiGaO_2$ was prepared by a solid state reaction using Li_2CO_3 (99.99%; Kojundo Chemical Laboratory) and Ga_2O_3 (99.99%;

* Corresponding author. Fax: +81 6879 7464.
E-mail address: omata@mat.eng.osaka-u.ac.jp (T. Omata).

0022-4596/$ - see front matter © 2012 Elsevier Inc. All rights reserved.
doi:10.1016/j.jssc.2012.01.053

Kojundo Chemical Laboratory) as the starting materials. The starting Li_2CO_3 and Ga_2O_3 were weighed in the molar ratio of $x(Li_2CO_3):x(Ga_2O_3)=1.06:1$ and mixed. The mixed powder was pressed into 17.2 mm diameter disks at 256 MPa, and then calcined at 600 °C for 48 h. The calcined disks were crushed and washed using ultrapure water in order to eliminate any excess and unreacted Li_2CO_3. The dried powder was pressed into disks, and then sintered at 1100 °C for 20 h. The obtained β-$LiGaO_2$ and ZnO (99.99%; Sigma–Aldrich) were weighed and mixed in the appropriate alloying ratio. The mixed powder was pressed into disks and calcined at 1000 °C for 20 h, then sintered at 1100 °C for 20 h.

The $LiGaO_2$ concentration, x, in $x(LiGaO_2)_{1/2}(1-x)ZnO$ was determined by inductively-coupled-plasma atomic emission spectrometry (ICP-AES; SII Nanotechnology SPS7800). The obtained crystalline phases were identified by powder XRD (Rigaku, RINT2500, Cu-K_α radiation using a curved graphite receiving monochromator). The SAD images using a 50-μm selector aperture were obtained using a transmission electron microscope (Hitachi H8100) operating at 200 kV. The Raman spectra of the samples were studied using an NRS-3100 laser Raman spectrometer (JASCO Co., Ltd.) at the 532 nm excitation wavelength. In order to obtain spectra that are not dependent on the crystal orientation, the spectra were recorded for an area of approximately 0.2 mm in diameter of the ceramic sample. We checked that the spectra did not change depending on the position in the specimen. The optical properties were studied by diffuse reflectance, photoluminescence (PL) and photoluminescence-excitation (PLE) spectroscopies. The diffuse reflectance spectra for the powdered sample were recorded by a double-beam spectrophotometer (Hitachi U4000) equipped with a white coated (MgO) integrating sphere. MgO powder was used as the reference material. The PL and PLE spectra were recorded by a JASCO FP6500 spectrometer using a monochromated xenon discharge lamp as the excitation light source.

3. Results and discussion

3.1. Structure of $x(LiGaO_2)_{1/2}(1-x)ZnO$

Fig. 1(a) and (b) shows the XRD profiles of the $x(LiGaO_2)_{1/2}(1-x)ZnO$ specimens. In Fig. 1(a), all the diffraction peaks were identified as those of the hexagonal wurtzite structure in the composition range of $x<0.2$. When the $LiGaO_2$ concentration increased to $x=0.20$, an extremely broadened diffraction appeared at $2\theta\sim22^\circ$ (indicated by the open circle in Fig. 1) in addition to the diffractions indexed as those of the hexagonal wurtzite phase. This extra diffraction became slightly sharper and its intensity increased with the increasing $LiGaO_2$ concentration. At the composition of $x=0.50$, the broad diffraction split into three diffractions at $2\theta=20.7$, 22.7 and 27.1° and many superlattice diffractions indicated by the open triangles appeared. The XRD profile accompanying by many superlattice diffractions was identified as that of the wurtzite-derived Zn_2LiGaO_4 as described in a previous paper [6]. From these observations, the extremely broadened diffraction at $2\theta\sim22^\circ$ for the sample with $0.2\le x\le0.5$ must be an indication of the start of cation-ordering. According to the additional experiments, in which the Zn_2LiGaO_4 samples were annealed at various temperatures and then it was quenched and supplied to XRD measurements, those superlattice diffractions diffused for the samples after annealing above 1000 °C, and the XRD profile became very similar to that of the sample with $0.2\le x\le0.4$ as indicated in Fig. 1(a); however, the diffused superlattice diffraction at $2\theta\sim22^\circ$ did not disappear for the sample annealed at 1400 °C. The results indicate that the cation-ordering develops in lower temperatures blow 1000 °C, and the ordering does not disappear even at as high temperature as 1400 °C.

Fig. 2 shows the SAD images of the sample with $0\le x\le0.5$. All the SAD patterns were recorded at the $\langle\bar{2}\,2\,1\rangle$ zone axis of the hexagonal wurtzite structure. For the samples with $x=0$ and 0.10,

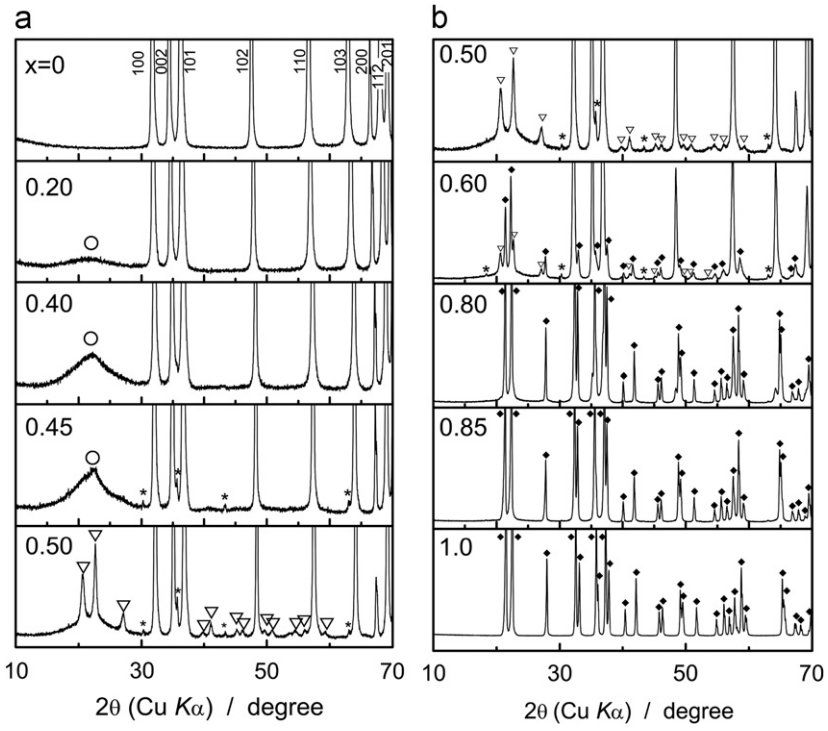

Fig. 1. Powder X-ray diffraction profiles of $x(LiGaO_2)_{1/2}(1-x)ZnO$ alloys. The open circles and triangles indicate diffuse diffraction and superlattice diffractions, respectively, due to cation-ordering of Zn, Li and Ga. The closed squares indicate the diffractions due to β-$LiGaO_2$ phase. The asterisks indicate $ZnGa_2O_4$ impurity.

intense diffractions that are indexed as ⟨1 1 0⟩,⟨1 0 2⟩ and ⟨0 1 $\bar{2}$⟩ based on the hexagonal wurtzite lattice were clearly observed. In the images for $x=0.20$ and 0.30, some faint and diffuse satellite spots indicated by the arrows in the images appeared in the direction of ⟨1 1 0⟩. For $x=0.40$, some satellite spots indicated by arrows were clearly observed in the direction of ⟨1 1 0⟩ in addition to the intense fundamental diffractions; and the position of the diffractions almost agreed with that for the Zn_2LiGaO_4 ($x=0.50$) [6].

For the composition of $0.5<x<0.8$, another set of diffractions indicated by the closed squares due to the β-$LiGaO_2$-type phase appeared in addition to the diffractions due to the Zn_2LiGaO_4 phase as shown in Fig. 1(b). This indicated that the mixture of the two phases of Zn_2LiGaO_4- and β-$LiGaO_2$-types is stable for $0.5<x<0.8$. Above $x\geq 0.8$, the β-$LiGaO_2$-type phase only appeared. Based on these XRD and SAD observations, the phases that appeared are the simple wurtzite-type phase for $0\leq x<0.2$, the cation-ordered Zn_2LiGaO_4- type phase for $0.2\leq x\leq 0.5$ and β-$LiGaO_2$-type phase for $0.8\leq x\leq 1$. The composition region of $0.5<x<0.8$ is two-phase region of the mixture of Zn_2LiGaO_4- and β-$LiGaO_2$-type phases.

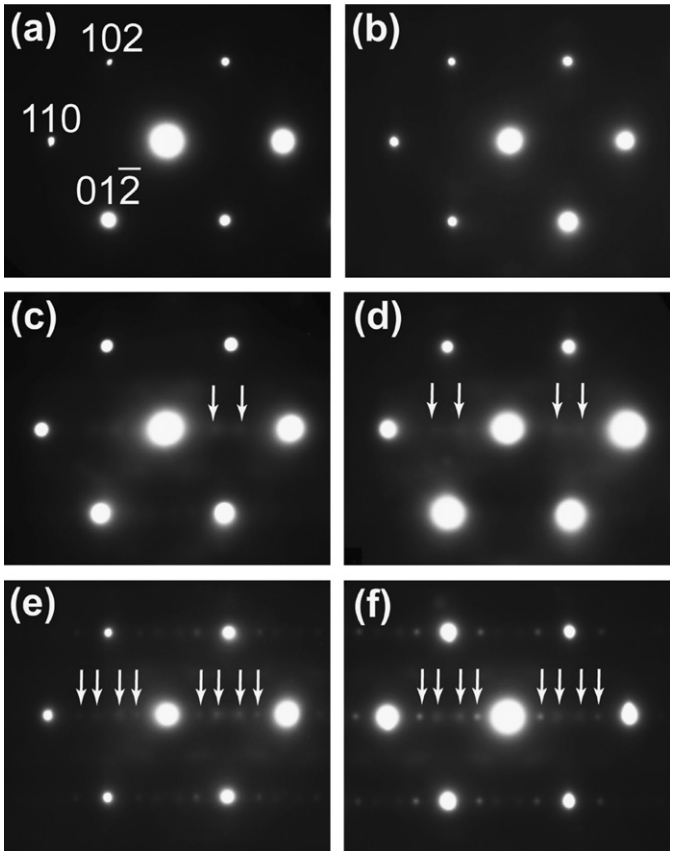

Fig. 2. TEM-SAD patterns of $x(LiGaO_2)_{1/2}(1-x)ZnO$ alloys of (a) $x=0$, (b) 0.10, (c) 0.20, (d) 0.30, (e) 0.40 and (f) 0.50. All the patterns were recorded at ⟨$\bar{2}$2 1⟩ zone axis of hexagonal wurtzite structure.

Fig. 3(a), (b) and (c) show variations in the lattice parameters and the c_0/a_0 ratio of the $x(LiGaO_2)_{1/2}(1-x)ZnO$ alloy system depending on the alloying level, x. For the lower $LiGaO_2$ concentration, the wurtzite-type phase was transformed into the cation-ordered Zn_2LiGaO_4-type phase above $x\geq 0.2$ as already described. The detailed structural parameters of the Zn_2LiGaO_4 phase are still unclear; therefore, we assumed the pseudo-hexagonal lattice for the Zn_2LiGaO_4 phase in the present study. In the wurtzite- and Zn_2LiGaO_4-type phase region, $0\leq x\leq 0.5$, both the lattice parameters, a_0 and c_0, decreased with the increasing $LiGaO_2$ concentration as indicated in Fig. 3(a). Because the average ionic radius of Li^+ and Ga^{3+} is 530 pm, and is smaller than that of Zn^{2+} (600 pm) [16], the lattice shrinkage upon replacing Zn with Li and Ga is definitely acceptable. In the $xMgO(1-x)ZnO$ system, the lattice parameter a_0 increases with the increasing alloying level, while c_0 decreases upon increasing the alloying level [17, 18]. Such a different behavior of the lattice parameters upon alloying between the $x(LiGaO_2)_{1/2}(1-x)ZnO$ and $xMgO(1-x)ZnO$ can be explained by the local structure of the MO_4 tetrahedra in the wurtzite structure as follows. Fig. 4 schematically shows the interatomic distances and bond angles of the MO_4 tetrahedra in the wurtzite structure (M=Zn and Mg) and wurtzite-derived β-$LiGaO_2$ structure (M=Li and Ga). In the wurtzite-type MgO phase evaluated by the DFT-LDA and DFT-GGA calculations [19, 20], the Mg atom significantly deviated from the center of the regular tetrahedron, and expanded the basal oxygen triangle in the *ab*-plane. According to the calculations study, the side length of the basal regular triangle for the MgO_4 tetrahedron is 326.1 pm from LDA and 338.2 pm from GGA that is slightly larger than that for ZnO_4, 324.9 pm, in the wurtzite ZnO [21]. On the contrary, the 246.9 pm (LDA) and 260.0 pm (GGA) heights of the MgO_4 tetrahedron (along the *c*-axis) is slightly smaller than that of 260.3 pm for ZnO_4. We expect the real parameters lie within the boundaries given by the LDA and GGA calculations. Therefore, the experimental observation in $xMgO(1-x)ZnO$ system that the substitution of Zn by Mg results in shrinkage of c_0 and expansion of a_0 can be explained based on the shape of the nearest neighbor tetrahedron of constituent cation.

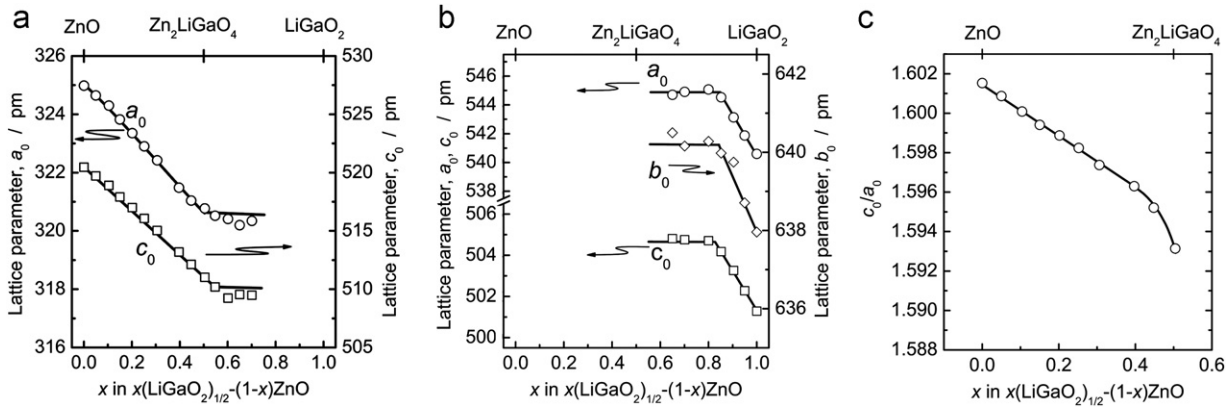

Fig. 3. Variation in lattice parameters of $x(LiGaO_2)_{1/2}(1-x)ZnO$ alloys depending on the $LiGaO_2$ concentration, x. (a) wurtzite and Zn_2LiGaO_4 phases, (b) β-$LiGaO_2$ phase and (c) c_0/a_0 for wurtzite and Zn_2LiGaO_4 phases. Hexagonal wurtzite lattice is assumed for the Zn_2LiGaO_4 phase. The β-$LiGaO_2$ phase is orthorhombic β-$LiGaO_2$ phase.

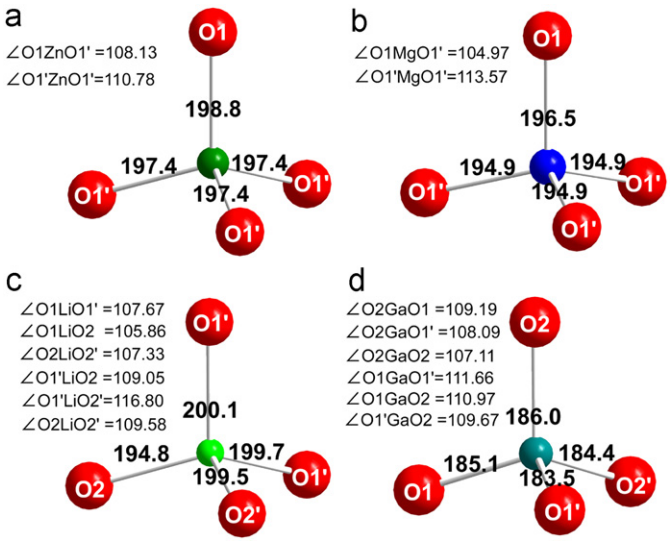

Fig. 4. Schematic illustration of (a) ZnO_4 and (b) MgO_4 tetrahedra in wurtzite phase and (c) LiO_4 and (d) GaO_4 in β-$LiGaO_2$ phase. The interatomic distances and angles in the tetrahedra are indicated in the figure. The MgO_4 tetrahedron is theoretically calculated in Ref. 19. The unit for the interatomic distance is picometer.

Table 1
Lattice parameters, a_0 and c_0, their ratio, c_0/a_0, and the oxygen parameter, u, for various wurtzite phases.

Compound	a_0	c_0	c_0/a_0	u	Ref.
AlN	311.117	498.017	1.6007	0.3866	23
ZnO	324.94	520.54	1.6020	0.3820	21
InN	353.77	570.37	1.6123	0.3769	29
BeO	269.79	437.72	1.6224	0.3786	24
CdS	413.70	671.44	1.6230	0.375	25
GaN	318.94	518.61	1.6260	0.3789	28
CdSe	429.82	700.84	1.6305	0.37586	26
ZnTe	427.3	698.9	1.6356	0.375	32
CdTe	457	748	1.637	0.375	27
ZnS	382.27	626.07	1.6378	0.3748	30
ZnSe	399.6	626.6	1.6582	0.375	31

For the GaO_4 and LiO_4 tetrahedra in β-$LiGaO_2$, the average side lengths of the basal triangle are 303.4 pm and 327.8 pm, respectively, and the heights of GaO_4 and LiO_4 are 239.4 pm and 261.3 pm, respectively [22]. These values indicate that the GaO_4 tetrahedron is 7–8% smaller in both the basal plane and height than ZnO_4, while the LiO_4 tetrahedron is almost the same size as ZnO_4. Therefore, the shrinkage of both the a_0 and c_0 upon the substitution of Zn by Li and Ga is reasonable from the viewpoint of the size of the coordination polyhedra.

We also observed the monotonic decrease in the c_0/a_0 ratio upon increasing the $LiGaO_2$ concentration in Fig. 3(c); the c_0/a_0 reached 1.593 at the solubility limit of $x=0.50$. Table 1 summarizes the c_0/a_0 values for the various binary wurtzite phases [21, 23–32]. The c_0/a_0 is 1.633 for the ideal wurtzite structure, and it ranges from 1.601 for AlN to 1.658 for ZnSe. There is no wurtzite compound with a c_0/a_0 lower than 1.6. For the polycrystalline and powdered xMgO$(1-x)$ZnO system reported by Kim et al., the c_0/a_0 decreased from 1.602 for $x=0$ to 1.600 for $x=0.15$ that is the solubility limit of MgO in ZnO [17]. Based on these results, the wurtzite structure, of which c_0/a_0 is lower than 1.6, is considered to be unstable. Because the c_0/a_0 ratio of 1.593 for the Zn_2LiGaO_4 is very close to 1.6, but is lower than 1.6, the solubility limit of $LiGaO_2$ in ZnO of $x=0.5$ may be phenomenologically understandable by the fact that the c_0/a_0 ratio decreased smaller than 1.6. Generally, the large anion position parameter, u, that is 0.375 for the ideal wurtzite structure, results in a lower c_0/a_0 ratio. It is very interesting whether or not the situation may be applicable to the present system. Consequently, the structural refinement of the Zn_2LiGaO_4 phase is strongly required in order to understand the solubility limit of $LiGaO_2$ in ZnO from a structural aspect, and we are now studying the detailed structure of Zn_2LiGaO_4.

For the higher $LiGaO_2$ concentration region ($0.8 \le x \le 1$), all the lattice parameters decreased with the increasing alloying level as indicated in Fig. 3(b). Such a variation is acceptable based on the ionic radii of the constituent cations as described above.

According to the previous studies of alloys of the cubic zincblende phase with a cation-ordered tetragonal chalcopyrite phase, such as the ZnSe–$CuInSe_2$ system, that is the chrcogenide analogy of the present ZnO–$LiGaO_2$ system, the two-phase region, in which the zincblende and chalcopyrite phases co-exist, usually appears except for ZnS–$CuM'S_2$ with M′=In, Ga and Al [8–14]. This situation is similar to the present ZnO–$LiGaO_2$ system; however, the presence of the cation-ordered I–II_2–III–VI_4 quaternary compound has not yet been reported for the zincblende and chalcopyrite alloy system. The presence of the cation-ordered Zn_2LiGaO_4 phase in the present system should originate from the higher ionicity of the oxide than the chalcogenides, i.e., the higher Madelung energy term.

3.2. Raman spectroscopy

Fig. 5 shows the Raman spectra of the $x(LiGaO_2)_{1/2}(1-x)$ZnO alloys. Upon the alloying of ZnO with $LiGaO_2$, most of the observed bands were broadened and the spectral intensity was significantly altered. However, the wurtzite ZnO-like optical phonons are only observed in $0 \le x \le 0.2$; Zn_2LiGaO_4-like and β-$LiGaO_2$-like optical phonons are observed in $0.2 \le x \le 0.5$ and

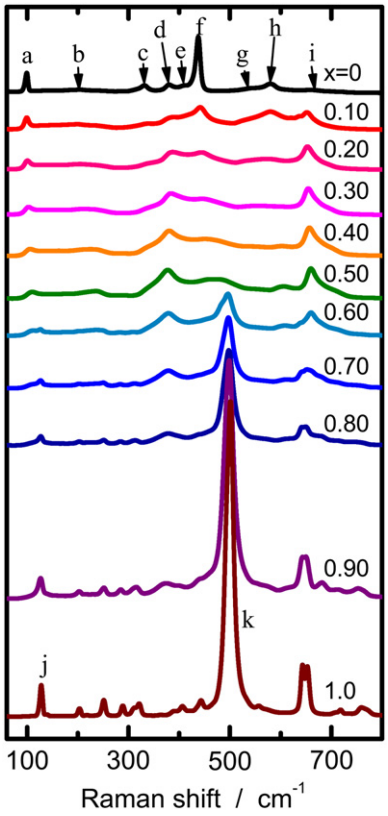

Fig. 5. Raman spectra of $x(LiGaO_2)_{1/2}(1-x)$ZnO alloys.

$0.8 \le x \le 1$, respectively. For $0.5 < x < 0.8$, both the β-$LiGaO_2$- and Zn_2LiGaO_4-like optical phonons appeared. These changes in the spectral features depending on the alloying level, x, support the structural variation evaluation based on the XRD and TEM-SAD observations.

In the Raman spectra of the alloyed semiconductors, optical phonons dependent on the composition are denoted by the one-mode or two-mode behavior [33, 34]. As seen in Fig. 5, the alloy systems of wurtzite- ($0 \le x < 0.2$), Zn_2LiGaO_4- ($0.2 \le x \le 0.5$) and β-$LiGaO_2$-type ($0.8 \le x \le 1$) exhibit a one-mode behavior in the respective alloy regions. The one-mode behavior in the wurtzite-type region of the present alloy agrees with the previously reported xMgO$(1-x)$ZnO alloy case [35]. The modified random-element-isodisplacement model gives an approximate prediction whether the ternary $AB_{1-x}C_x$ or $A_{1-x}B_xC$ alloys exhibit a one-mode or two-mode behavior [36]. According to the phenomenological model, the alloy exhibiting the one-mode behavior must not have one substituting element whose mass, m, is smaller than the reduced mass, μ, of the compound formed by the other two elements. As an example of the $A_{1-x}B_xC$ alloy,

$$m_B > \mu_{AC} \text{ and } m_A > \mu_{BC} \quad (1)$$

where $\mu_{AC}=m_Am_C/(m_A+m_C)$ and $\mu_{BC}=m_Bm_C/(m_B+m_C)$. In the xMgO$(1-x)$ZnO alloy case, its one-mode behavior was explained by meeting the above condition (1). Returning to the present pseudo-binary $x(LiGaO_2)_{1/2}(1-x)$ZnO alloy case, when the average mass, $m_{Li,Ga}$, is assumed to be $0.5m_{Li}+0.5m_{Ga}$, the relationships between the atomic mass and reduced mass are

$$m_{Li,Ga} = 36.2 > \mu_{ZnO} = 12.84 \text{ and } m_{Zn} = 65.39 > \mu_{(LiGaO_2)1/2} = 11.1 \quad (2)$$

The one-mode behavior is expected from the relationships, and it is consistent with the observed behavior of the alloys.

We next discuss the shift in the optical phonon frequency upon changing the alloying level. The group theory predicts the following Γ-point optical phonons for the wurtzite structure. $A_1+E_1+2E_2+2B_1$, which are all Raman active except for the silent B_1 modes [37]. According to previous studies, the observed Raman bands a–i for the pure ZnO in Fig. 5 are attributed to the respective modes as summarized in Table 2 [38–41], and the atomic motions for the Raman active A_1, E_1 and E_2 modes are schematically shown in Fig. 6 [42]. Fig. 7 shows the composition dependence of the Raman shift of bands a, d and f. For the bands a and f attributed to the E_2^{low} and E_2^{high} modes, the Raman shifts increased with the increasing x. The vibrations corresponding to both the E_2^{low} and E_2^{high} modes are associated with the atomic motions in the ab-plane as shown in Fig. 6. In the present alloy system, both the a- and c-axes shrank with the increasing alloying level, x. This suggests that the bond strength for the MO_4 tetrahedra increases with the increasing alloying level. Therefore, the blue-shift in the E_2^{low} and E_2^{high} modes is reasonably understood. In addition, the replacement of Zn with Li and Ga decreases the reduced mass as described by Eq. (2); it reasonably increases the energy of the vibrations. In the xMgO$(1-x)$ZnO case, the reduced mass is also decreased by the substitution of Zn by Mg, but the E_2^{high} mode exhibited a red-shift upon increasing the light Mg concentration. Such a situation was explained by the phonon softening caused by the in-plane lattice expansion as

Table 2
Assignments of characteristic Raman modes for pure ZnO (x=0).

Band	Raman shift (cm^{-1})	Mode
a	99	E_2^{low}
b	203	E_2^{low}(m)[a]
c	331	E_2^{low}(m)
d	380	A_1(TO)
e	409	E_1(TO)
f	438	E_2^{high}
g	541	E_2^{low}(m)
h	579	A_1(LO), E_1(LO)
i	657	E_2^{low}(m)

[a] E_2^{low}(m) indicates multi-phonon scattering related to E_2^{low} mode.

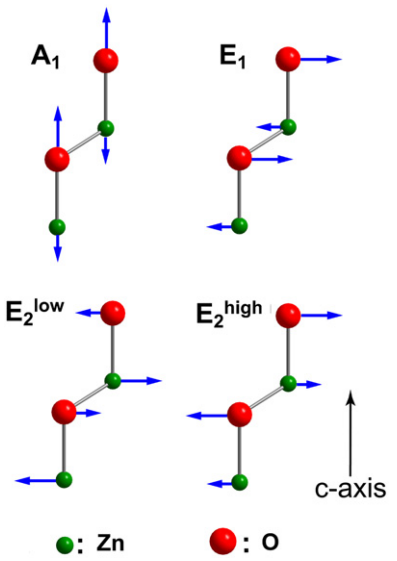

Fig. 6. Schematic illustration of atomic motions for the Raman active optical modes A_1, E_1 and E_2^{low} and E_2^{high} for wurtzite structure.

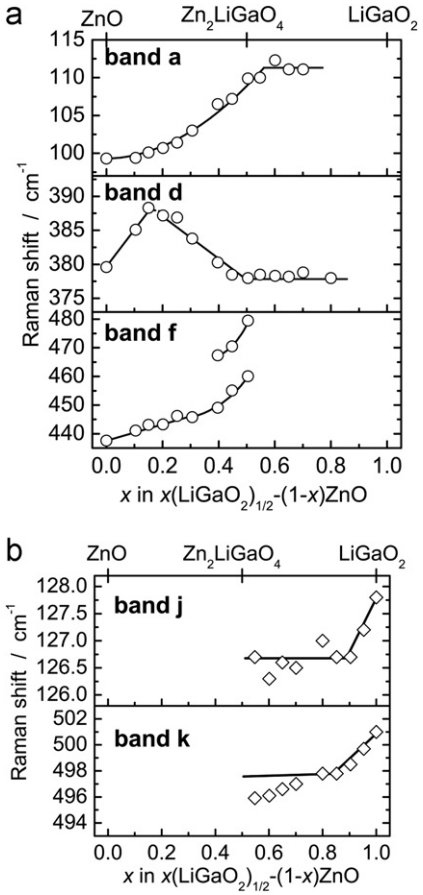

Fig. 7. Variation in the Raman shift for the a, d, f, j and k bands of the alloy depending on the $LiGaO_2$ concentration x in $x(LiGaO_2)_{1/2}(1-x)$ZnO.

reported by Kim et al. [43]. However, in the present case, both the *a*- and *c*-axes decreased with the increasing alloying level, *x*; therefore we do not have to consider the condition, such as the phonon softening, in the wurtzite-type $x(LiGaO_2)_{1/2}(1-x)ZnO$ alloys unlike the $xMgO(1-x)ZnO$ alloys.

The d band that is attributable to the $A_1(TO)$ mode associated with the atomic motion parallel to the *c*-axis exhibited a blue-shift in the wurtzite phase region ($x<0.2$). The blue-shift is explained by the same situation for the E_2^{low} and E_2^{high} modes as described above. The band exhibited a red-shift in the Zn_2LiGaO_4 region ($0.2\le x\le 0.5$). The red-shift may be due to the partial cation-ordering effect. In the Raman spectra for the higher $LiGaO_2$ concentration region of the Zn_2LiGaO_4 phase ($0.4\le x\le 0.5$), the f band is clearly split into two bands. Of course, the splitting should be due to the lower symmetry of the Zn_2LiGaO_4 structure than the wurtzite structure. The structural refinement of the Zn_2LiGaO_4 phase is definitely expected in order to provide a more detailed discussion.

For the β-$LiGaO_2$ phase, Kabelka et al. studied the Raman spectrum of the β-$LiGaO_2$ phase and indicated that the *Γ*-point optical phonons for this phase is $11A_1+12A_2+11B_1+11B_2$ [44, 45]. Recently, Boonchun and Lanbrecht theoretically studied the vibrational mode and reported that the k band attributed to the A_1 mode corresponds to the atomic motions in the *ab*-plane similar to the E_2^{high} mode for the wurtzite phase [46]. The j band should also correspond to the motions in the *ab*-plane because of its very close energy to the E_2^{low} mode of the wurtzite phase. Both the j and k bands exhibited a blue shift with the increasing $LiGaO_2$ concentration, *x*, in the β-$LiGaO_2$ phase region ($0.8\le x\le 1$). This situation is also explained by the lattice shrinkage and the reduction of the reduced mass upon substitution of Zn with Li and Ga.

The Raman shifts of the bands indicated in Fig. 7 are dependent on the alloying level in $0\le x\le 0.5$ and $0.8\le x\le 1$, and they are almost constant in $0.5<x<0.8$. This observation strongly supports the phase variation evaluated on the basis of the XRD and TEM-SAD observations.

3.3. UV–Vis and PL spectra

Fig. 8 shows the diffuse reflectance spectra in the UV–Vis region of $x(LiGaO_2)_{1/2}(1-x)ZnO$ with $0\le x\le 0.5$. For the pure ZnO ($x=0$), the onset of reflectance was observed at ~380 nm that corresponds to the fundamental absorption edge. With the increasing $LiGaO_2$ concentration to $x=0.10$, the absorption edge slightly shifts to the longer wavelength region, although the shift was very small. The red-shift is an indication of band gap bowing. A further increase in the $LiGaO_2$ concentration greater than $x=0.10$ resulted in a blue-shift of the absorption edge up to ~310 nm for $x=0.50$, i.e., Zn_2LiGaO_4. Fig. 9(a) and (b) shows the PL and PLE spectra of the alloys. In the PL spectra, a broad visible emission for the pure ZnO centered at 580 nm is attributable to the electron-hole pair recombination via the Li-acceptor level according to previous studies [47, 48]. The band exhibited a red-shift up to $x=0.10$ and a blue-shift for $x>0.1$ similar to that observed in the UV–Vis spectra. In the PLE spectra of the visible emission (Fig. 9(b)), we observed a clear local maximum that is explained as the inter-band transition of the electron from the valence band to the conduction band, i.e., the energy of the local maximum corresponds to the energy band gap of the alloys. The maximum is located at 367 nm (3.38 eV) for ZnO ($x=0$) and at 307 nm (4.04 eV) for Zn_2LiGaO_4 ($x=0.50$); these energies agree well with the energy band gap of the pure ZnO and Zn_2LiGaO_4 [1–6]. Fig. 10 shows the energy band gap that is determined based on the PLE of the alloys depending on the $LiGaO_2$ concentration. In the figure, pure ZnO and Zn_2LiGaO_4 are employed as terminal components. The energy band gap of the intermediate composition slightly deviated downward from the linear relationship as indicated by the dashed line, for instance, band gap bowing is clearly observed. However, the bowing is not very significant as compared to $xBeO(1-x)ZnO$ and the other II–VI alloys. Generally, the energy band gap of a pseudo-binary alloyed semiconductor, such as the present $y(Zn_2LiGaO_4)_{1/4}(1-y)ZnO$ is described by

$$E_g(y)=yE_g(Zn_2LiGaO_4)+(1-y)E_g(ZnO)-b(1-y)y \quad (3)$$

where $E_g(Zn_2LiGaO_4)$ and $E_g(ZnO)$ are the energy band gaps of 4.04 and 3.38 eV for Zn_2LiGaO_4 and ZnO, respectively, and *b* is the optical bowing parameter [49]. From the fitting our data to Eq. (3) (solid line in Fig. 10), the bowing parameter was determined to be

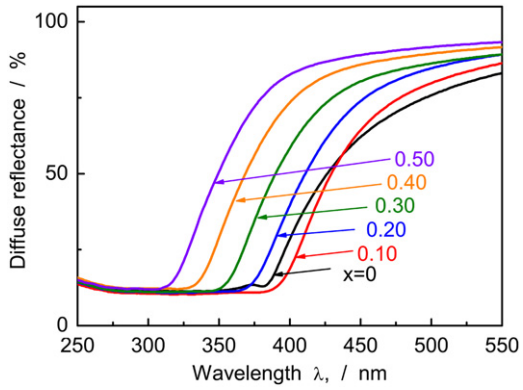

Fig. 8. UV–Vis diffuse reflectance spectra of $x(LiGaO_2)_{1/2}(1-x)ZnO$ alloys.

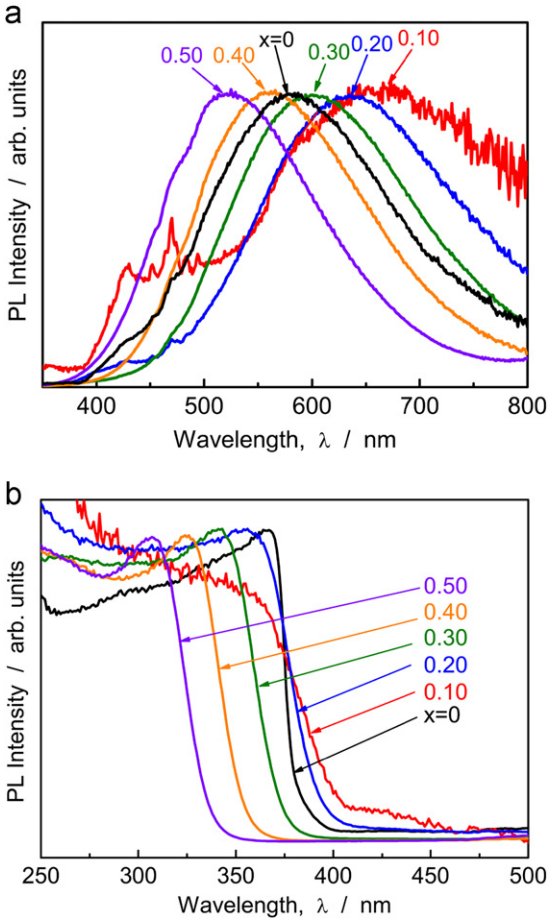

Fig. 9. (a) PL and (b) PLE spectra of $x(LiGaO_2)_{1/2}(1-x)ZnO$ alloys for $0\le x\le 0.5$.

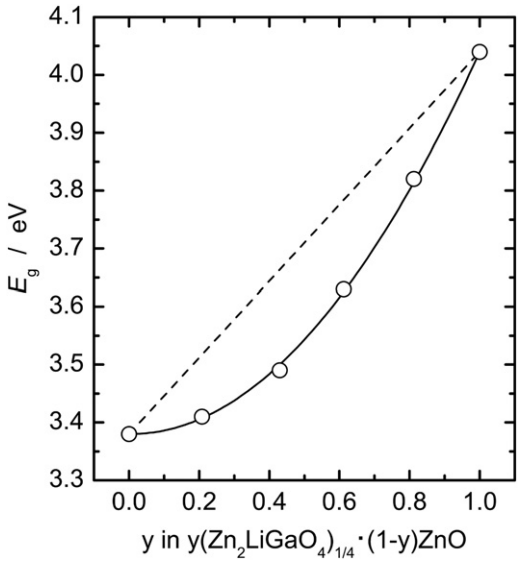

Fig. 10. Variation in optical band gap of $y(Zn_2LiGaO_4)_{1/4}(1-y)$ZnO alloys for $0 \le x \le 0.5$. The solid line indicates the curve calculated using $E_g = 3.38(1-y) + 4.04y - 0.67y(1-y)$.

0.67 eV. This value is very close to that for xMgO$(1-x)$ZnO, 0.8–0.9 eV [50–52], and much lower than that for xBeO$(1-x)$ZnO, 5.6 eV [53], and the other II–VI alloys, 2–20 eV [49]. The magnitude of the bowing is usually related to the lattice mismatch and band offset (chemical mismatch) [49]. The lattice parameters a_0 and c_0 for ZnO are 325.0 and 520.5 pm, respectively, and for Zn_2LiGaO_4, they are 320.8 and 511.0 pm as shown in Fig. 3. These values show that the lattice mismatch of the two phases is less than 2%.

Because the band offset between the ZnO and Zn_2LiGaO_4 has not been clarified at this time, a theoretical discussion regarding the band offset is given here. The valence bands for these two phases are mainly composed of the oxygen 2p component. This means that the energies of the valence band for the two phases should be close. Consequently, the valence band offset is expected to be small. The difference in the energy band gap between the ZnO and Zn_2LiGaO_4 is only 0.66 eV; the situation suggests that the conduction band offset is not very significant when taking the small valence band offset into account. Thus, both the valence and conduction band offsets are expected to be small in addition to the small lattice mismatch. The small band gap bowing is a natural consequence based on these situations.

4. Summary

Structural variation of the $x(LiGaO_2)_{1/2}(1-x)$ZnO alloy system was studied by powder XRD and TEM-SAD. It was elucidated that the phase that appeared in the system varied upon increasing the alloying level as the wurtzite-type from $0 \le x < 0.2$, the Zn_2LiGaO_4-type from $0.2 \le x \le 0.5$ and the β-$LiGaO_2$-type from $0.8 \le x \le 1$. The intermediate composition of $0.5 < x < 0.8$ is a mixture of the Zn_2LiGaO_4 and β-$LiGaO_2$ phases. In the low $LiGaO_2$ concentration region, the hexagonal c_0/a_0 ratio decreased to 1.593 for Zn_2LiGaO_4 ($x = 0.50$). The solubility limit of $LiGaO_2$ in ZnO is phenomenologically explained by the low c_0/a_0 ratio based on the fact that there is no binary wurtzite phase with a c_0/a_0 value less than 1.6. The optical phonons studied by Raman spectroscopy in the system were explained by the lattice shrinkage and the reduced mass reduction upon the alloying of ZnO with $LiGaO_2$. No special condition, such as a phonon softening, has to be considered unlike the MgO–ZnO system. Based on the UV–Vis and PL spectroscopies, the bowing parameter of the optical band gap of $y(Zn_2LiGaO_4)_{1/4}(1-y)$ZnO was determined to be 0.67 eV. Such a small bowing parameter was related to the small lattice and chemical mismatches between the Zn_2LiGaO_4 and ZnO. For further detailed analyses of the structural and optical properties of the present alloy system, a structural analysis of the Zn_2LiGaO_4 is strongly required.

Acknowledgment

This work was supported in part by a Grant-in-Aid for Scientific Research of Challenging Exploratory Research (Grant No. 23656402).

References

[1] Ü. Özgür, Y.I. Alivov, C. Liu, A. Teko, M.A. Reshchikov, S. Doğan, V. Avrutin, S.-J. Cho, H. Morkoç, J. Appl. Phys. 98 (2005). 041301/1-103.
[2] A. Ohtomo, M. Kawasaki, T. Koida, K. Masubuchi, H. Koinuma, Y. Sakurai, Y. Yoshida, T. Yasuda, Y. Segawa, Appl. Phys. Lett. 72 (1988) 2466–2468.
[3] T. Makino, Y. Segawa, M. Kawasaki, A. Ohtomo, R. Shiroki, K. Tamura, T. Yasuda, H. Koinuma, Appl. Phys. Lett. 78 (2001) 1237–1238.
[4] J.F.H. Nicholls, H. Gallangher, B. Henderson, C. Trager-Cowan, P.G. Middleton, and L.P. O'Donnell, Mater. Res. Soc. Symp. Proc. 395 (1996) pp. 535–539.
[5] T. Omata, K. Tanaka, A. Tazuke, K. Nose, S. Otsuka-Yao-Matsuo, J. Appl. Phys. 103 (2008). 083706/1-4.
[6] T. Omata, M. Kita, K. Nose, K. Tachibana, S. Otsuka-Yao-Matsuo, Jpn. J. Appl. Phys. 50 (2011). 031102/1-4.
[7] T. Omata, K. Tanaka, S. Otsuka-Yao-Matsuo, Jpn. J. Appl. Phys. 50 (2011). 061102/1-6.
[8] V. Riede, H. Neumann, N. Sharif, F.S. Hasoon, H. Sobatta, Phys. Status Solidi A 112 (1989) K139–143.
[9] M. Robbins, M.A. Miksovsky, J. Solid State Chem. 5 (1972) 462–466.
[10] P. Grima-Gallardo, M. Munoz, J. Ruiz, C. Power, J. Gonzalez, Y. LeGodec, P. Munsch, J.P. Itie, V. Briceno, J.M. Briceno, Phys. Status Solidi B 241 (2004) 1795–1802.
[11] E.F. Apple, J. Electrochem. Soc. 105 (1958) 251–255.
[12] J.N. Gan, J. Tauc, V.G. Lambrecht Jr., M. Robbins, Phys. Rev. B 12 (1975) 5797–5802.
[13] P.G. Gallardo, Phys. Status Solidi A 130 (1992) 39–44.
[14] V.O. Halka, I.D. Olekseyuk, O.V. Parasyuk, J. Alloys Compd. 302 (2000) 173–176.
[15] Y.R. Ryu, T.S. Lee, J.A. Lubguban, A.B. Corman, H.W. White, J.H. Leem, M.S. Han, Y.S. Park, C.J. Youn, W.J. Kim, Appl. Phys. Lett. 88 (2006). 052103/1-2.
[16] R.D. Shannon, Acta Crystallogr., Sect. A: Found. Crystallogr. 32 (1976) 751–767.
[17] Y.-I. Kim, K. Page, R. Seshadri, Appl. Phys. Lett. 90 (2007). 101904/1-3.
[18] Y.-I. Kim, S. Cadars, R. Shayib, T. Proffen, C.S. Feigerle, B.F. Chemelka, R. Seshadri, Phys. Rev. B: Condens. Matter 78 (2008). 195205/1-11.
[19] A. Janotti, D. Segev, C.G.Vande Walle, Phys. Rev. B: Condens. Matter 74 (2006). 045202/1-9.
[20] M. Heinemann, M. Giar, C. Heiliger, MRS Proceedings 1201(2010)1201-H05-33.
[21] H. Sowa, H. Ahsbahs, J. Appl. Crystallogr. 39 (2006) 169–175.
[22] M. Marezio, Acta Crystallogr., Sect. A: Found. Crystallogr. 18 (1965) 481–484.
[23] K. Nakahigashi, H. Ishibashi, S. Minamigawa, J. Phys. Chem. Solids 54 (1993) 445–452.
[24] D.K. Smith Jr., H.W. Newkivk, J.S. Kahn, J. Electrochem. Soc. 111 (1964) 78–87.
[25] Y.-N. Xu, W.Y. Ching, Phys. Rev. B: Condens. Matter 48 (1993) 4335–4351.
[26] H. Sowa, Solid State Sci. 7 (2005) 1384–1489.
[27] S.A. Semiletov, Trudy Inst. Kristallogr. Akad. Nauk SSSR 11 (1955) 121–123.
[28] W. Paszkowicz, S. Podsiadlo, R. Minikayev, J. Alloys Compd. 382 (2004) 100–106.
[29] W. Paszkowicz, R. Cerny, S. Krukowski, Powder Diffr. 18 (2003) 114–121.
[30] E.H. Kisi, M.M. Elcombe, Acta Crystallogr., Sect. C: Cryst. Struct. Commun. 45 (1989) 1867–1870.
[31] I.V. Korneeva, Sov. Phys. Crystallogr. 6 (1961) 505–506.
[32] C. Yeh, Z.W. Lu, S. Froyen, A. Zunger, Phys. Rev. B: Condens. Matter 46 (1992) 10086–10097.
[33] C.S. Yang, W.C. Chou, D.M. Chen, C.S. Ro, J.L. Shen, T.R. Yang, Phys. Rev. B: Condens. Matter 59 (1999) 8128–8131.
[34] D.J. Lockwood, Z.R. Wasilewski, Phys. Rev. B: Condens. Matter 70 (2004). 155202/1-9.
[35] Z.P. Wei, Y.M. Lu, D.Z. Shen, Z.Z. Zhang, C.X. Wu, J.Y. Zhang, B. Yao, X.W. Fan, Phys. Status Solidi C 3 (2006) 1168–1171.
[36] I.F. Chang, S.S. Mitra, Phys. Rev. 172 (1968) 924–933.
[37] C.A. Arguello, D.L. Rousseau, S.P.S. Porto, Phys. Rev. 181 (1969) 1351–1363.
[38] T.C. Damen, S.P.S. Porto, B. Tell, Phys. Rev. 142 (1966) 570–574.
[39] J.M. Calleja, M. Cardona, Phys. Rev. B: Condens. Matter 16 (1977) 3753–3761.
[40] N. Ashkenov, B.N. Mbeukum, C. Bundesmann, V. Riede, M. Lorenz, D. Spemann, E.M. Kaidashev, A. Kasic, M. Schubert, M. Grundmann,

G. Wagner, H. Neumann, V. Darakchieva, H. Arwin, B. Monemar, J. Appl. Phys. 93 (2003) 126–133.
[41] H.W. Kunert, Phys. Status Solidi C 1 (2004) 206–212.
[42] H. Harima, J. Phys. Condens. Matter 14 (2002) R967–993.
[43] Y.-I. Kim, K. Page, A.M. Limarga, D.R. Clarke, R. Seshadri, Phys. Rev. B: Condens. Matter 76 (2007). 115204/1-10.
[44] P. Knoll, H. Kuzmany, Phys. Rev. B: Condens. Matter 29 (1984) 2221–2226.
[45] H. Kabelka, H. Kuzmany, P. Kremple, Solid State Commun. 27 (1978) 1159–1162.
[46] A. Boonchun, W.R.L. Lanbrecht, Phys. Rev. B: Condens. Matter 81 (2010). 235214/1-12.
[47] O.F. Schirmer, D. Zwingel, Solid State Commun. 8 (1970) 1559–1563.
[48] N. Ohashi, T. Nakata, T. Sekiguchi, H. Hosono, M. Mizuguchi, T. Tsurumi, J. Tanaka, H. Haneda, Jpn. J. Appl. Phys. 38 (1999) L113–115.
[49] C.-Y. Moon, S.-H. Wei, Y.Z. Zhu, G.D. Chen, Phys. Rev. B: Condens. Matter 74 (2006). 233202/1-4.
[50] Y.-S. Chang, C.-T. Chien, C.-W. Chen, T.-Y. Wu, C.-S. Lin, L.C.-C. Chen, K.-H. Chen, J. Appl. Phys. 101 (2007). 033502/1-7.
[51] H.-L. Shi, Y. Duan, Eur. Phys. J. B 66 (2008) 439–444.
[52] X.F. Fan, H.D. Sun, Z.X. Shen, J.-L. Kuo, Y.M. Lu, J. Phys. Condens. Matter 20 (2008). 235221/1-9.
[53] S.F. Ding, G.H. Fan, S.T. Li, K. Chen, B. Xiao, Physica B 394 (2007) 127–131.